

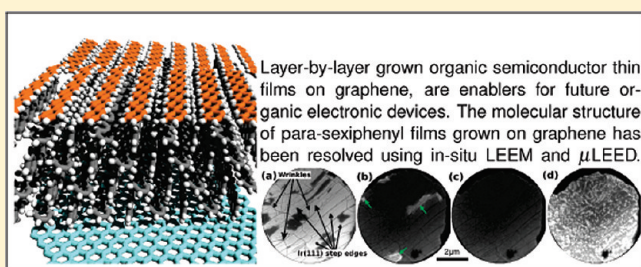
# Smooth Growth of Organic Semiconductor Films on Graphene for High-Efficiency Electronics

Gregor Hlawacek,<sup>\*,†,‡</sup> Fawad S. Khokhar,<sup>†</sup> Raoul van Gastel,<sup>†</sup> Bene Poelsema,<sup>†</sup> and Christian Teichert<sup>‡</sup>

<sup>\*</sup>Physics of Interfaces and Nanomaterials, MESA<sup>+</sup> Institute for Nanotechnology, University of Twente, P.O. Box 217, NL-7500AE, Enschede, The Netherlands

<sup>†</sup>Institute for Physics, University of Leoben, Franz Josef Strasse 18, A-8700 Leoben, Austria

**ABSTRACT:** High-quality thin films of conjugated molecules with smooth interfaces are important to assist the advent of organic electronics. Here, we report on the layer-by-layer growth of the organic semiconductor molecule *p*-sexiphenyl (6P) on the transparent electrode material graphene. Low energy electron microscopy and micro low energy electron diffraction reveal the morphological and structural evolution of the thin film. The layer-by-layer growth of 6P on graphene proceeds by subsequent adding of  $\{\overline{1}\overline{1}\}$  layers.



**KEYWORDS:** Graphene, organic semiconductor, layer-by-layer growth, low-energy electron microscopy, low-energy electron diffraction

Smooth interfaces are a prerequisite for future, high-performance, and low-cost organic electronic devices<sup>1</sup> based on small conjugated molecules. The quality of the first few layers is of critical importance since all important charge transport processes are confined to the first two or three monolayers (ML).<sup>2</sup> However, often these films grow in a three-dimensional manner resulting in rough surfaces.<sup>3–7</sup> To obtain sufficient smoothness at the interface, it is a prerequisite that the active region is formed in a layer-by-layer growth mode. The resulting flat interfaces exhibit a lower number of defects and generally yield a higher charge carrier mobility.<sup>8–11</sup> We have achieved this goal for *p*-sexiphenyl (6P) molecules on graphene. Layer-by-layer growth of lying 6P molecules on metal-supported graphene flakes is realized. The formation of several layers has been monitored *in situ* by means of low energy electron microscopy (LEEM). Micro low energy electron diffraction ( $\mu$ LEED) has been used to reveal a bulklike structure of the submonolayer, monolayer, and multilayer regime. The combination of the established deposition technique organic molecular beam deposition (OMBD) with the unique properties of organic semiconductors and graphene is a viable route for future flexible and cost efficient devices based on small conjugated molecules. On the one hand, 6P is a blue light emitter with a high charge carrier mobility<sup>12</sup> that makes it well suited for the fabrication of organic light emitting diodes. On the other hand, graphene is a flexible, highly conductive, and transparent electrode material,<sup>13,14</sup> ideally suited as a technological substrate for organic semiconductors.<sup>15,16</sup> For the present study graphene flakes on Ir(111) were used as they show only weak coupling to the underlying substrate<sup>17</sup> and can be grown with millimeter size.<sup>18</sup> A transparent substrate and layer-by-layer growth of lying molecules are the perfect combination for high output color tunable organic light emitting diodes.<sup>19</sup>

Single layer graphene sheets were grown on an Ir(111) surface.<sup>20</sup> The metal crystal was cleaned by high temperature

exposure to O<sub>2</sub>. The graphene layer was then formed by thermal decomposition of ethylene on the hot (875 K) Ir(111) surface.<sup>18</sup> The growth of graphene was followed in real time using photo emission electron microscopy (PEEM) until sufficiently large flakes had formed on the surface. Using  $\mu$ LEED the orientation of the graphene flakes was verified. Only flakes that are aligned with the substrate were selected for analysis during and after the deposition of 6P.<sup>18</sup> The sample was then cooled to 240 K before deposition of 6P by OMBD from a resistively heated Knudsen cell evaporator designed for the deposition of organic molecules. The sublimation purified source material has been purchased from TCI Europe N.V. Care was taken to remove remaining low boiling point contaminations by a thorough outgassing of the evaporator for several hours prior to the experiment. The film formation was followed *in situ* using an Elmitec LEEM III. Images were recorded every second at typical energies of 2 eV, well below the band gap of 3.1 eV for 6P. The film structure was investigated using the *in situ*  $\mu$ LEED capabilities of the instrument. All  $\mu$ LEED measurements were carried out at the deposition temperature of 240 K using a field limiting aperture with a projected diameter of 1.4  $\mu$ m.

Figure 1 shows a sequence of LEEM images taken during growth of the first four monolayers of 6P on graphene. Figure 1a shows a graphene flake and the first 6P islands that nucleated after 134 s of deposition. Thin undulated lines correspond to steps of the supporting Ir(111) substrate. The more pronounced straight thick lines stem from wrinkles in the graphene layer.<sup>21,22</sup> While the islands do not grow over the wrinkles, they do cross the steps of the underlying Ir. After roughly 400 s of growth (not shown) a second, darker level of contrast becomes visible in the center of the existing 6P islands. Eventually the initial layer (1514 s

**Received:** July 21, 2010

**Published:** January 5, 2011

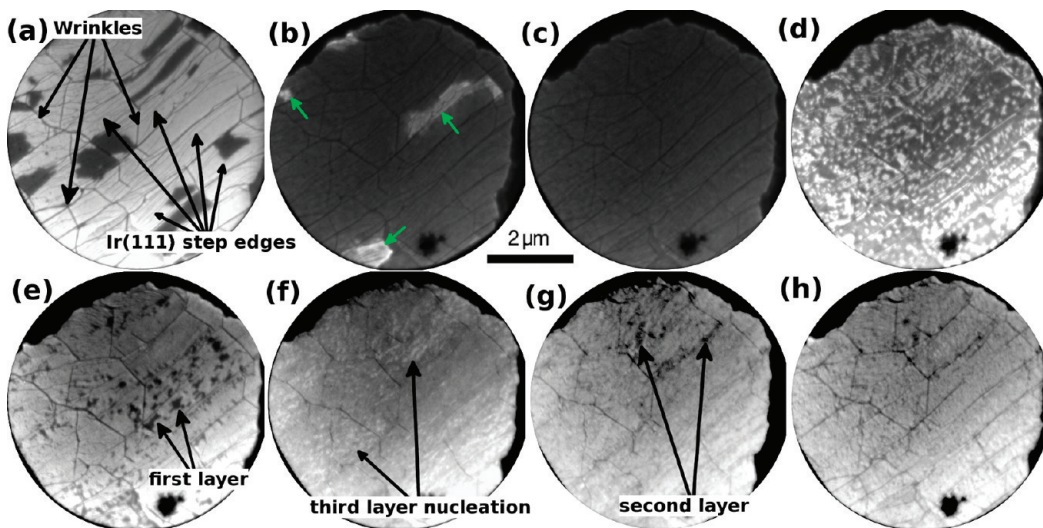


**Figure 1.** 6P layer-by-layer growth on graphene. Sequence of LEEM images taken during the growth of the first three monolayers of 6P on graphene. The field of view (FOV) is  $6\text{ }\mu\text{m}$  in all images. (a,  $t = 134\text{ s}$ ) Graphene flake with Ir steps and wrinkles. Steps appear as narrow undulated lines, whereas the straight wrinkles appear as wider lines rotated by  $60^\circ$  with respect to each other. Dark areas are islands that have nucleated next to the wrinkles. (b,  $t = 1514\text{ s}$ ) The islands visible in (a) have formed a closed initial layer (medium gray, marked by arrows). From  $400\text{ s}$  onward a second, darker contrast develops on top of the initial layer. This full first monolayer (dark gray) is nearly completed. (c,  $t = 1698\text{ s}$ ) The first monolayer is now completed. The wrinkles are still visible. (d,  $t = 2107\text{ s}$ ) Nucleation of the second layer (bright areas) is observed simultaneously in random positions on the graphene flake. (e,  $t = 2901\text{ s}$ ) The second layer is nearly closed. (f,  $t = 3467\text{ s}$ ) The cycle repeats with the formation of the third layer (bright areas). (g,  $t = 4429\text{ s}$ ) The third layer is nearly closed. (h,  $t = 5723\text{ s}$ ) Another cycle, corresponding to the growth of the fourth layer, starts. The dark spot in the lower part of all images is a defect in the micro channel plate of the LEEM. All images have been adjusted for optimum contrast.

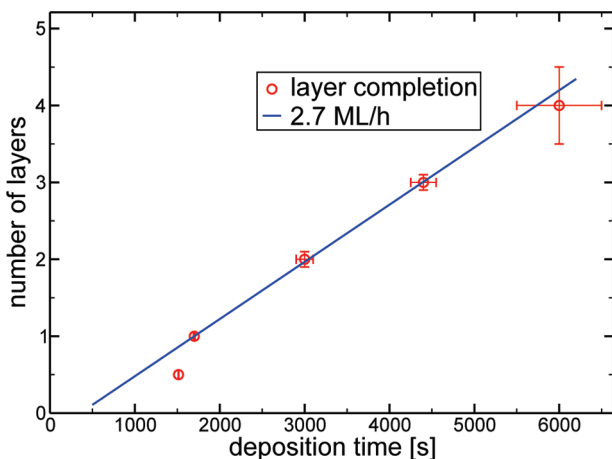


**Figure 2.** Layer completion times. All but the first data point correspond to the closing of a full monolayer of 6P. From the linear fit (ignoring the first data point) a growth rate of  $2.7\text{ ML/h}$  is obtained.

of 6P growth, medium gray, marked by arrows) has closed (Figure 1b). Only  $184\text{ s}$  later the second darker area covers the whole surface (Figure 1c). In Figure 1d, bright islands are observed to form. They eventually coalesce (Figure 1e), leading to a uniform contrast. This cycle then repeats with the nucleation of another set of islands (Figure 1f). After some time, the contrast becomes uniform again (see Figure 1g), indicating the completion of the next layer. Figure 1h shows the start of the next repetition of this cycle.

Figure 2 shows the temporal distribution of the formation of fully closed layers. Using all but the first data point, which corresponds to the closing of the initial layer, we find a growth rate of  $2.7\text{ ML/h}$ . Here, we use the term monolayer for a closed layer of molecules having the final structure. The layer-by-layer

growth is therefore followed for four complete layers, the structure of which will be discussed next.

The structure of the 6P layers was characterized by  $\mu$ LEED. Figure 3 shows two LEED patterns obtained during the formation of the first complete layer of 6P on graphene. The measured unit cell is  $a = 28.1\text{ \AA}$  and  $b = 6.0\text{ \AA}$ , with  $\beta = 79^\circ$  and  $\Theta = 79^\circ$  for the initial layer (Figure 3a) that yields a medium gray contrast in Figure 1a,b. Here,  $a$  and  $b$  denote the long and short unit cell axis,  $\beta$  is the angle between them, and  $\Theta$  is the angle between the long side  $a$  and the [1000] zigzag direction of the graphene layer. From the size of the unit cell, it is immediately evident that the film is formed by one flat-lying molecule per unit cell, i.e., molecules where the average orientation of the benzene rings is parallel to the substrate. Contrary to what has been observed for 6P on highly oriented pyrolytic graphite,<sup>23</sup> the molecules are not aligned with the [1100] armchair direction of graphene. Instead, a similar, loosely packed open structure with a matrix notation of

$$\begin{bmatrix} 8.7 & 13.0 \\ -1.3 & 1.5 \end{bmatrix}$$

is found (Figure 3c). The long axis (LA) of the molecule is parallel to the [0120] direction of graphene (corresponds to rotation by  $11^\circ$  with respect to graphite), while the short axis (SA) is  $3^\circ$  off the [2010] direction. Assuming an on-top position for the first phenyl ring, the fourth phenyl ring will have a similar position. This metastable structure only exists in the initial stage of the formation of a layer. Why it is different might be related to the unique structure of graphene. Little is known about the adsorption of organic molecules on graphene. However, recent studies on benzene adsorption reveal a net Mulliken charge transfer of  $0.03\text{ e}$  from the molecule to the graphene.<sup>24</sup> In addition the same study reveals a weaker binding of benzene to graphene

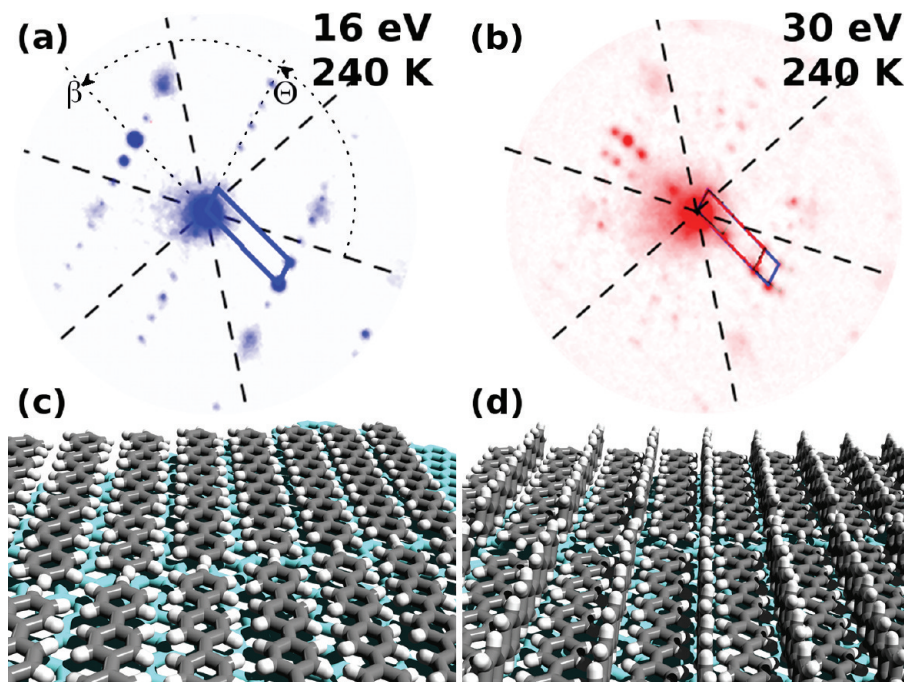


**Figure 3.** Submonolayer and monolayer structure. (a)  $\mu$ LEED pattern obtained from the first half and (b) the completed first layer. Dashed lines indicate the [1000] (zigzag) direction of the graphene flake. The angles  $\beta$  and  $\Theta$  used for the description of the unit cells are indicated. Panels (c) and (d) show the proposed structure of the first half and full first layer. (In (c) and (d) planar molecules are used for clarity.)

( $E_b = 0.24$  eV) compared to values reported for graphite ( $E_b = 0.35$  eV).<sup>25</sup> As a first estimate for 6P on graphene, these values can be multiplied by 6 to achieve the correct order of magnitude.

To shed more light on the difference in adsorption geometry, some basic molecular dynamic simulations have been performed. Single 6P molecules have been placed on sufficiently large pieces of either single or double layer (to simulate graphite) graphene. A variant<sup>26</sup> of the Tripos-5.2 force field<sup>27</sup> has been used for these calculations in combination with the molecular modeling software Avogadro.<sup>28</sup> All four possible configurations have been allowed to relax until the change between two successive steps was less than a fraction of  $10^{-8}$  of the total energy. The obtained total energies were compared to the sum of the total energies of the molecule and the substrate. Comparing the calculated binding energies, the case of the LA of 6P parallel to the (01 $\bar{2}0$ ) direction of graphene ( $LA_{6P\parallel}(01\bar{2}0_{graphene})$ ) is favored (by  $\approx 300$  meV) on graphene while the LA of 6P parallel to the [10 $\bar{1}0$ ] direction ( $LA_{6P\parallel}(10\bar{1}0_{graphene})$ ) is favored (by  $\approx 100$  meV) for the double layer graphene sheet. These results perfectly agree with the observations by Wang et al.<sup>23</sup> for 6P on graphite and those made in the current paper for 6P on graphene.

After roughly 400 s of 6P film growth, a second more dense structure starts to form, resulting in the LEED pattern presented in Figure 3b and corresponding to the dark gray contrast in the LEEM images (see Figure 1b,c). The unit cell size increases to  $a = 28.1$  Å,  $b = 7.5$  Å,  $\beta = 69^\circ$ , and  $\Theta = 79^\circ$  with matrix notation:

$$\begin{bmatrix} 8.7 & 13.0 \\ -1.7 & 1.9 \end{bmatrix}$$

(two molecules per unit cell). The only way to accommodate the additional 6P molecules is in an edge-on configuration, interdigitating the flat-lying molecules. In addition, some of the former flat-lying molecules will need to tilt into an edge-on configuration

as well. The energy gain due to the higher mismatch—compared to the completely flat lying initial layer—is more than compensated by the positive effect of a bulklike arrangement of the molecules already in the first monolayer (Figure 3d). A similar structure and growth mechanism for the first monolayer of 6P has been observed on Au(111).<sup>29</sup>

Figure 4a shows a  $\mu$ LEED pattern that was obtained from a 4.35 ML 6P film on graphene. Two unit cells can be identified. Several weak spots can be attributed to a unit cell with a size of  $a = 26.9$  Å,  $b = 9.2$  Å, with  $\beta = 74^\circ$  and  $\Theta = 77^\circ$ . A second smaller unit cell has the dimensions:  $a = 6.8$  Å,  $b = 6.4$  Å, with  $\beta = 75^\circ$  and  $\Theta = 141^\circ$ . Keeping the amount of deposited 6P in mind, we interpret the former as a bulk continuation of what was observed for the first layer. This unit cell is similar to the surface unit cell of the bulk 6P{111} plane.<sup>30</sup> This bulklike unit cell with a size of 236.7 Å<sup>2</sup> holds two molecules. Figure 4b shows spot profiles along the (11)-direction of the spot labeled O(11) for different energies (extracted from the  $\mu$ LEED patterns). Such spot profiles are the result of a regular step train in two layers, i.e., single layer islands of equal size in a regular arrangement.<sup>31</sup> From the spot splitting we infer an island size of 28.7 Å, implying that the 6P molecules themselves give rise to the spot-splitting. Therefore, the smaller of the two unit cells is associated with diffraction from the ordered phenyl rings that constitute the 6P molecule. Using the measured positions for the phenyl rings, a unit cell for the molecules can be derived with a size of  $a = 29.2$  Å,  $b = 6.3$  Å, with  $\beta = 75^\circ$  and  $\Theta = 0^\circ$ . Here,  $\Theta$  is given with respect to the long unit cell axis of the underlying bulk 6P. One molecule is contained in this unit cell, which has an area of 162.7 Å<sup>2</sup> and a matrix notation of

$$\begin{bmatrix} 1.1 & 0 \\ 0 & 0.7 \end{bmatrix}$$

with respect to the underlying 6P. This overlayer is aligned with the underlying bulk 6P but only every 11 and 7 molecules along the long

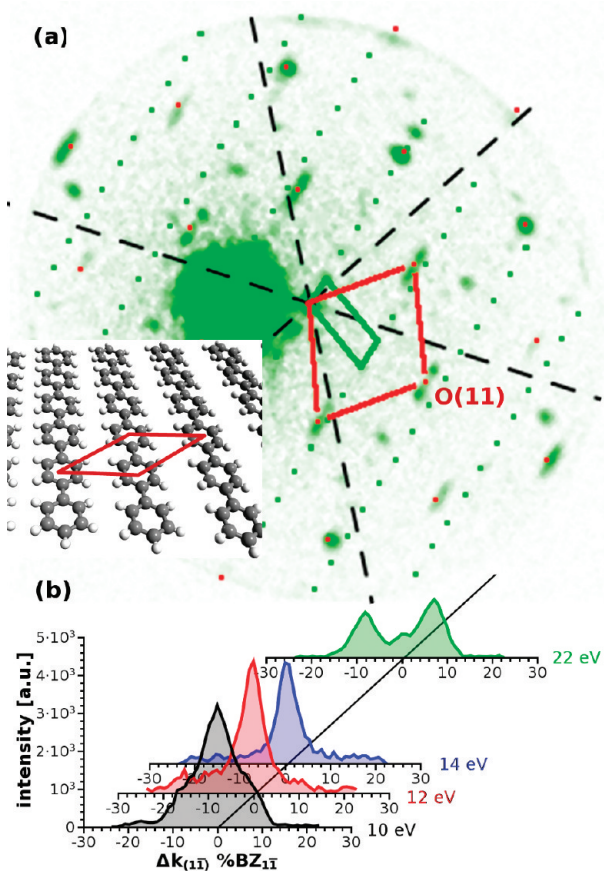


**Figure 4.**  $\mu$ LEED pattern obtained from a 4.5 ML thick 6P film on graphene. (a) The measured unit cell parameters for the green cell are  $a = 26.9 \text{ \AA}$ ,  $b = 9.2 \text{ \AA}$ , with  $\beta = 74^\circ$  and  $\Theta = 77^\circ$ . The red unit cell with a size of  $a = 6.8 \text{ \AA}$ ,  $b = 6.4 \text{ \AA}$ , with  $\beta = 75^\circ$  and  $\Theta = 141^\circ$ , results from diffraction of the individual phenyl rings. The inset shows the real space structure of the adlayer together with the unit cell (solid red line). (b) Spot profiles of the O(11)-spot belonging to the red unit cell in panel (a). The profiles for different electron energies have been shifted to enhance visibility.

and short axis direction respectively will be in the same position. As a result of the lower molecular density in the adlayer, 50% of the surface is covered by this adlayer. The measured energy dependence of the spot profile (see Figure 4b) allows the thickness of the adlayer to be estimated. Using  $2d = n\lambda$  for the in phase condition (at 14 eV) and  $2d = (n + (1/2))\lambda$  for the out of phase condition (at 22 eV), we can calculate a value of  $n = 2$  (1.97).<sup>32</sup> The resulting spacing between the adlayer and the uppermost flat molecules of the bulk 6P is then 3.3 Å. The distance between two  $\{1\bar{1}\}$  planes in the bulk is 4.6 Å.<sup>30</sup> Figure 5 shows the proposed structure for the full stack of molecules. Four layers of bulklike 6P (gray carbon atoms) with the  $\{1\bar{1}\}$  plane parallel to the underlying graphene sheet (light blue carbon atoms for clarity) are covered by an adlayer of only flat lying molecules (orange carbon atoms).

In conclusion, using LEEM, we have demonstrated the growth of atomically smooth layers of the organic semiconductor 6P on a graphene substrate. Initially, small islands are formed. An open structure consisting of only flat-lying molecules was found as an initial structure for the first layer with  $\mu$ LEED. This layer then transforms into a complete monolayer through the addition of interdigitating, edge-on molecules, that result in a bulklike arrangement of the molecules. Subsequent layers are formed by a

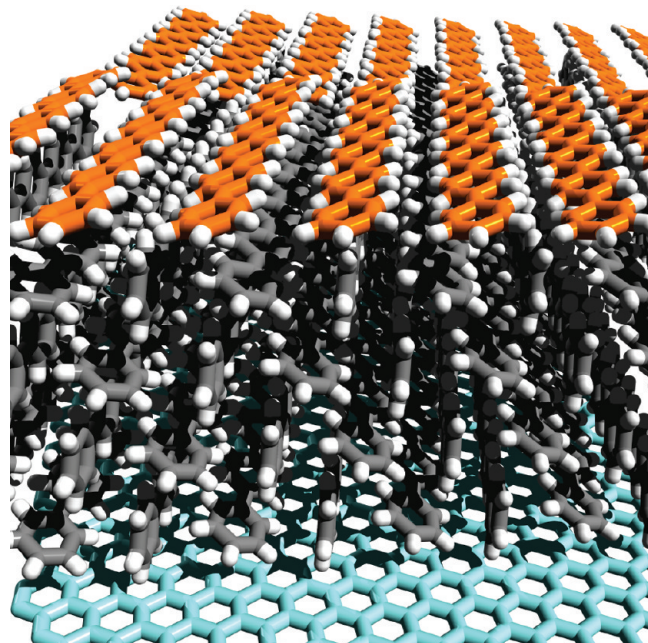


**Figure 5.** Proposed structure of 6P on metal supported graphene. Four Layers of bulklike 6P are deposited with their  $\{1\bar{1}\}$  plane parallel to the graphene substrate (light blue carbon atoms for clarity). The adlayer covering 50% of the top surface is shown with orange carbon atoms.

repetition of this cycle, as we find an adlayer, with an open structure similar to what was found for the initial layer, covering the surface of thicker films. Up to at least 4.35 ML the growth continues in this layer-by-layer fashion. This growth mode will lead to films with a high charge carrier mobility and good overall device performance. As such it is an enabler for future organic, flexible, and low-cost devices.<sup>33</sup>

## ■ AUTHOR INFORMATION

### Corresponding Author

\*E-mail: g.hlawacek@tnw.utwente.nl

## ■ ACKNOWLEDGMENT

Help from Dmitrii Nabok in evaluating the molecular dynamics simulation is acknowledged. This work was financially supported by FWF project N9707-N20, STW, and FOM project 04PR2318.

## ■ REFERENCES

- (1) Chiang, C. K.; Fincher, C. R.; Park, Y. W.; Heeger, A. J.; Shirakawa, H.; Louis, E. J.; Gau, S. C.; MacDiarmid, A. G. *Phys. Rev. Lett.* **1977**, *39*, 1098–1101.
- (2) Dodabalapur, A.; Torsi, L.; Katz, H. E. *Science* **1995**, *268*, 270–271.
- (3) Dürr, A. C.; Schreiber, F.; Ritley, K. A.; Kruppa, V.; Krug, J.; Dosch, H.; Struth, B. *Phys. Rev. Lett.* **2003**, *90*, No. 016104.
- (4) Kowarik, S.; Gerlach, A.; Sellner, S.; Schreiber, F.; Pflaum, J.; Cavalcanti, L.; Konovalov, O. *Phys. Chem. Chem. Phys.* **2006**, *8*, 1834–1836.
- (5) Mikami, T.; Yanagi, H. *Appl. Phys. Lett.* **1998**, *73*, 563–565.
- (6) Hlawacek, G.; Puschnig, P.; Frank, P.; Winkler, A.; Ambrosch-Draxl, C.; Teichert, C. *Science* **2008**, *321*, 108–111.
- (7) Smilgies, D. M.; Kintzel, E. J. *Phys. Rev. B* **2009**, *79*, No. 235413.

- (8) Fritz, S. E.; Kelley, T. W.; Frisbie, C. D. *J. Phys. Chem. B* **2005**, *109*, 10574–10577.
- (9) Steudel, S.; De Vusser, S.; De Jonge, S.; Janssen, D.; Verlaak, S.; Genoe, J.; Heremans, P. *Appl. Phys. Lett.* **2004**, *85*, 4400–4402.
- (10) Yan, H.; Swaraj, S.; Wang, C.; Hwang, I.; Greenham, N. C.; Groves, C.; Ade, H.; McNeill, C. R. *Adv. Funct. Mater.* **2010**, *20*, 4329–4337.
- (11) Schumacher, D.; Stark, D. *Surf. Sci.* **1982**, *123*, 384–396.
- (12) Singh, T.; Hernandez-Sosa, G.; Neugebauer, H.; Andreev, A.; Sitter, H.; Sariciftci, N. S. *Phys. Status Solidi B* **2006**, *243*, 3329–3332.
- (13) Geim, A. K.; Novoselov, K. S. *Nat. Mater.* **2007**, *6*, 183–191.
- (14) Echtermeyer, T. J.; Lemme, M. C.; Baus, M.; Szafranek, B. N.; Geim, A. K.; Kurz, H. *IEEE Electron Device Lett.* **2008**, *29*, 952–954.
- (15) Lauffer, P.; Emtevse, K. V.; Graupner, R.; Seyller, T.; Ley, L. *Phys. Status Solidi B* **2008**, *245*, 2064–2067.
- (16) Wang, Q. H.; Hersam, M. C. *Nat. Chem.* **2009**, *1*, 206–211.
- (17) Pletikosić, I.; Kralj, M.; Pervan, P.; Brako, R.; Coraux, J.; N'Diaye, A. T.; Busse, C.; Michely, T. *Phys. Rev. Lett.* **2009**, *102*, No. 056808.
- (18) van Gastel, R.; N'Diaye, A. T.; Wall, D.; Coraux, J.; Busse, C.; Buckanie, N. M.; Meyer zu Heringdorf, F. J.; von Hoegen, M. H.; Michely, T.; Poelsema, B. *Appl. Phys. Lett.* **2009**, *95*, No. 121901.
- (19) Tasch, S.; Brandstaetter, C.; Meghdadi, F.; Leising, G.; Froyer, G.; Athouel, L. *Adv. Mater.* **1997**, *9*, 33–36.
- (20) Coraux, J.; N'Diaye, A. T.; Busse, C.; Michely, T. *Nano Lett.* **2008**, *8*, 565–570.
- (21) N'Diaye, A. T.; Gastel, R.; Martínez-Galera, A. J.; Coraux, J.; Hattab, H.; Wall, D.; Meyer zu Heringdorf, F. J.; Hoegen, M. H.; Gómez-Rodríguez, J. M.; Poelsema, B.; Busse, C.; Michely, T. *New J. Phys.* **2009**, *11*, No. 113056.
- (22) Loginova, E.; Nie, S.; Thürmer, K.; Bartelt, N. C.; McCarty, K. F. *Phys. Rev. B* **2009**, *80*, No. 085430.
- (23) Wang, Z. H.; Kanai, K.; Iketaki, K.; Ouchi, Y.; Seki, K. *Thin Solid Films* **2008**, *S16*, 2711–2715.
- (24) Zhang, Y.-H.; Zhou, K.-G.; Xie, K.-F.; Zeng, J.; Zhang, H.-L.; Peng, Y. *Nanotechnology* **2010**, *21*, No. 065201.
- (25) Fisher, A. J.; Blöchl, P. E. *Phys. Rev. Lett.* **1993**, *70*, 3263–3266.
- (26) OBForceFieldGhemical, 2010. <http://openbabel.org/wiki/OBForceFieldGhemical/>.
- (27) Hassinen, T.; Peräkylä, M. J. *Comput. Chem.* **2001**, *22*, 1229–1242.
- (28) Avogadro, version 1.0.0, 2010; <http://avogadro.openmolecules.net/>.
- (29) Müllegger, S.; Winkler, A. *Surf. Sci.* **2006**, *600*, 1290–1299.
- (30) Baker, K. N.; Fratini, A. V.; Resch, T.; Adams, W. W.; Socciand, E. P.; Farmer, B. L. *Polymer* **1993**, *34*, 1571–1587.
- (31) Henzler, M. *Appl. Surf. Sci.* **1982**, *11–12*, 450–469.
- (32) Henzler, M. *Surf. Sci.* **1970**, *19*, 159–171.
- (33) Gundlach, D. J. *Nat. Mater.* **2007**, *6*, 173–174.